FINAL REPORT FOR ONR GRANT N00014-16-1-2335
SCATTERING FROM ROCKS AND ROCK OUTCROPS
DISTRIBUTION A - APPROVED FOR PUBLIC RELEASE

DEREK R. OLSON

Applied Research Laboratory
The Pennsylvania State University

1. Long-Term Goals

In terms of target detection and classification, scattering from exposed rock on the seafloor, (i.e., individual rocks and rock outcrops) presents some of the most difficult challenges for modern MCM and ASW sonar systems in shallow water. Work on characterizing, modeling and simulating mean levels, and other statistical measures of acoustic scattering from rocks and rock outcrops is therefore critical. Unfortunately (and curiously) information on scattering from underwater rock and outcrops is almost non-existent. Scattering from rock outcrops is not simple enough to be encompassed by a single scattering strength curve, but has a variety of expressions depending on the exact geomorphology of the rock. Smoothed surfaces may actually scatter less than surrounding sediment; curvature may dramatically affect scattering and rough areas as seen on the rock outcrop in Fig. 1, display high variability which could pose difficulty for target detection and classification systems.

The primary long-term goal of this research project is to increase understanding and modeling capabilities for high-frequency acoustic scattering from rock and rock outcrops. In addition to an increase in basic understanding of the characteristics of scattering from rock, any resulting advances in modeling would be useful for improving simulation capabilities and for improving detection and classification tools. Inverse models based on forward models would be essential for using sonar systems for remote sensing of seafloor properties. An understanding of spatial coherence functions for isotropic and anisotropic rough seafloor surfaces could allow a method for separating natural 'target'-like objects such as rough rock from man-made targets.

2. Objectives

Our objectives for the proposed study of scattering from rocky seafloors and rock outcrops are intended to address many of the open questions which exist for scattering from these types of surfaces and include increasing our basic understanding of:

(1) geoacoustic characteristics of rock relevant to scattering,
(2) scattering strength versus grazing angle, and
(3) scattering statistics of rock outcrops.

Date: January 23, 2018.

REPORT DOCUMENTATION PAGE

Form Approved
OMB No. 0704-0188

1. REPORT DATE *(DD-MM-YYYY)*	2. REPORT TYPE	3. DATES COVERED *(From - To)*
23-01-2018	Final	02/24/2016 through 09/30/2017

4. TITLE AND SUBTITLE
Scattering from Rock and Rock Outcrops

5a. CONTRACT NUMBER

5b. GRANT NUMBER
N00014-16-1-2335

5c. PROGRAM ELEMENT NUMBER

6. AUTHOR(S)
Derek Olson

5d. PROJECT NUMBER
24571

5e. TASK NUMBER

5f. WORK UNIT NUMBER

7. PERFORMING ORGANIZATION NAME(S) AND ADDRESS(ES)
The Pennsylvania State University Applied Research Labotatory
Office of Sponsored Programs
110 Technology Center Building
University Park, PA 16802-7000

8. PERFORMING ORGANIZATION REPORT NUMBER

9. SPONSORING/MONITORING AGENCY NAME(S) AND ADDRESS(ES)
Office of Naval Research
875 North Randolph Street
Arlington, VA 22203-1995

10. SPONSOR/MONITOR'S ACRONYM(S)
BD025

11. SPONSORING/MONITORING AGENCY REPORT NUMBER

12. DISTRIBUTION AVAILABILITY STATEMENT
DISTRIBUTION A - APPROVED FOR PUBLIC RELEASE, distribution iss Unlimited

13. SUPPLEMENTARY NOTES

14. ABSTRACT
In terms of target detection and classification, scattering from exposed rock on the seafloor, (i.e., individual rocks and rock outcrops) presents some of the most difficult challenges for modern MCM and ASW sonar systems in shallow water. Work on characterizing, modeling and simulating mean levels, and other statistical measures of acoustic scattering from rocks and rock outcrops is therefore critical. Unfortunately information on scattering from underwater rock and outcrops is almost non-existent. The primary long-term goal of this research project is to increase understanding and modeling capabilities for high-frequency acoustic scattering from rock and rock outcrops. In addition to an increase in basic understanding of the characteristics of scattering from rock, any resulting advances in modeling would be useful for improving simulation capabilities and for improving detection and classification tools.

15. SUBJECT TERMS

16. SECURITY CLASSIFICATION OF:			17. LIMITATION OF ABSTRACT	18. NUMBER OF PAGES	19a. NAME OF RESPONSIBLE PERSON
a. REPORT	b. ABSTRACT	c. THIS PAGE	unlimited	15	Derek Olson
u	u	u			19b. TELEPONE NUMBER (*Include area code*) 814-863-9895

INSTRUCTIONS FOR COMPLETING SF 298

1. REPORT DATE. Full publication date, including day, month, if available. Must cite at lest the year and be Year 2000 compliant, e.g., 30-06-1998; xx-08-1998; xx-xx-1998.

2. REPORT TYPE. State the type of report, such as final, technical, interim, memorandum, master's thesis, progress, quarterly, research, special, group study, etc.

3. DATES COVERED. Indicate the time during which the work was performed and the report was written, e.g., Jun 1997 - Jun 1998; 1-10 Jun 1996; May - Nov 1998; Nov 1998.

4. TITLE. Enter title and subtitle with volume number and part number, if applicable. On classified documents, enter the title classification in parentheses.

5a. CONTRACT NUMBER. Enter all contract numbers as they appear in the report, e.g. F33615-86-C-5169.

5b. GRANT NUMBER. Enter all grant numbers as they appear in the report, e.g. 1F665702D1257.

5c. PROGRAM ELEMENT NUMBER. Enter all program element numbers as they appear in the report, e.g. AFOSR-82-1234.

5d. PROJECT NUMBER. Enter al project numbers as they appear in the report, e.g. 1F665702D1257; ILIR.

5e. TASK NUMBER. Enter all task numbers as they appear in the report, e.g. 05; RF0330201; T4112.

5f. WORK UNIT NUMBER. Enter all work unit numbers as they appear in the report, e.g. 001; AFAPL30480105.

6. AUTHOR(S). Enter name(s) of person(s) responsible for writing the report, performing the research, or credited with the content of the report. The form of entry is the last name, first name, middle initial, and additional qualifiers separated by commas, e.g. Smith, Richard, Jr.

7. PERFORMING ORGANIZATION NAME(S) AND ADDRESS(ES). Self-explanatory.

8. PERFORMING ORGANIZATION REPORT NUMBER. Enter all unique alphanumeric report numbers assigned by the performing organization, e.g. BRL-1234; AFWL-TR-85-4017-Vol-21-PT-2.

9. SPONSORING/MONITORS AGENCY NAME(S) AND ADDRESS(ES). Enter the name and address of the organization(s) financially responsible for and monitoring the work.

10. SPONSOR/MONITOR'S ACRONYM(S). Enter, if available, e.g. BRL, ARDEC, NADC.

11. SPONSOR/MONITOR'S REPORT NUMBER(S). Enter report number as assigned by the sponsoring/ monitoring agency, if available, e.g. BRL-TR-829; -215.

12. DISTRIBUTION/AVAILABILITY STATEMENT. Use agency-mandated availability statements to indicate the public availability or distribution limitations of the report. If additional limitations/restrictions or special markings are indicated, follow agency authorization procedures, e.g. RD/FRD, PROPIN, ITAR, etc. Include copyright information.

13. SUPPLEMENTARY NOTES. Enter information not included elsewhere such as: prepared in cooperation with; translation of; report supersedes; old edition number, etc.

14. ABSTRACT. A brief (approximately 200 words) factual summary of the most significant information.

15. SUBJECT TERMS. Key words or phrases identifying major concepts in the report.

16. SECURITY CLASSIFICATION. Enter security classification in accordance with security classification regulations, e.g. U, C, S, etc. If this form contains classified information, stamp classification level on the top and bottom of this page.

17. LIMITATION OF ABSTRACT. This block must be completed to assign a distribution limitation to the abstract. Enter UU (Unclassified Unlimited) or SAR (Same as Report). An entry in this block is necessary if the abstract is to be limited.

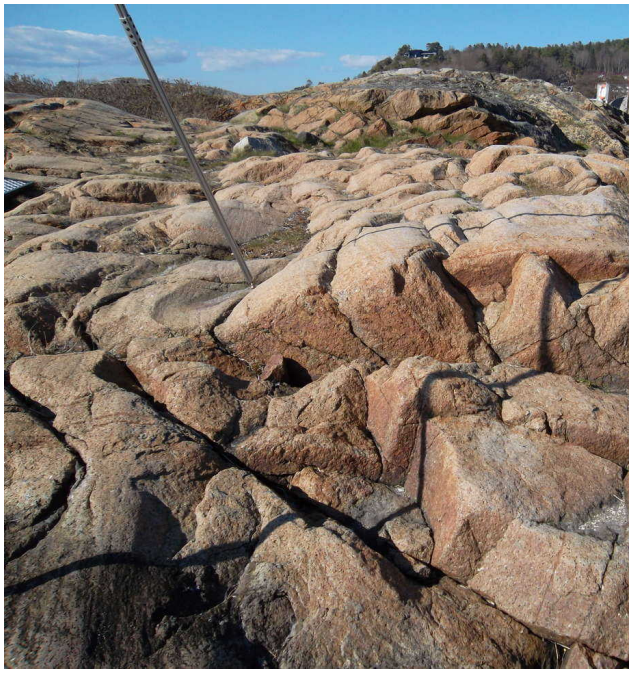

FIGURE 1. Photo of rock outcrop in the Oslofjord near Larvik, Norway. The outcrop is similar to underwater outcrops from which acoustic scattering was collected.

These goals were achieved through examination of existing literature, analysis of field data or lab measurements and by the use of extended approximate or numerical scattering models.

3. Work Completed

3.1. **Geoacoustic Properties of rock outcrops.** As virtually no information exists on scattering from rock outcrops, we have worked on obtaining relevant physical characteristics of rock outcrops, such as the geoacoustic properties, roughness, and morphology for use in models of acoustic scattering from rock. This year the methods developed in previous years to estimate scattering strength from SAS data were applied to a wider set of data and reported in [1].

The historical literature was examined to determine the mineral composition of the bedrock in the area. These data [2] were used to estimate the compressional wave speed, shear wave speed, and density of rock outcrops based on Hashin-Walpole-Shtrikman bounds [3]. These measurements in conjunction with effective medium theory resulted in estimates 6393 m/s for the compressional wave speed, 3276 m/s for the shear wave speed, and 2708 kg/m3 for the bulk density. To provide estimates of interface roughness, an experiment was performed in May 2013 using stereo photogrammetry. Both of these types of environmental ground truth were used to compute approximate scattering models that are compared with measured data. Analysis of these data reported in [1].

Roughness results from the May 2013 experiment are presented in Fig. 2 and Fig. 3 of abraded and plucked surfaces respectively. The terms abraded and plucked are discussed below. The root-mean-square (RMS) roughness of the abraded surface is 2.09 mm, and 45 mm for the plucked surface. These quantities correspond to values of 0.86 and 18 respectively.

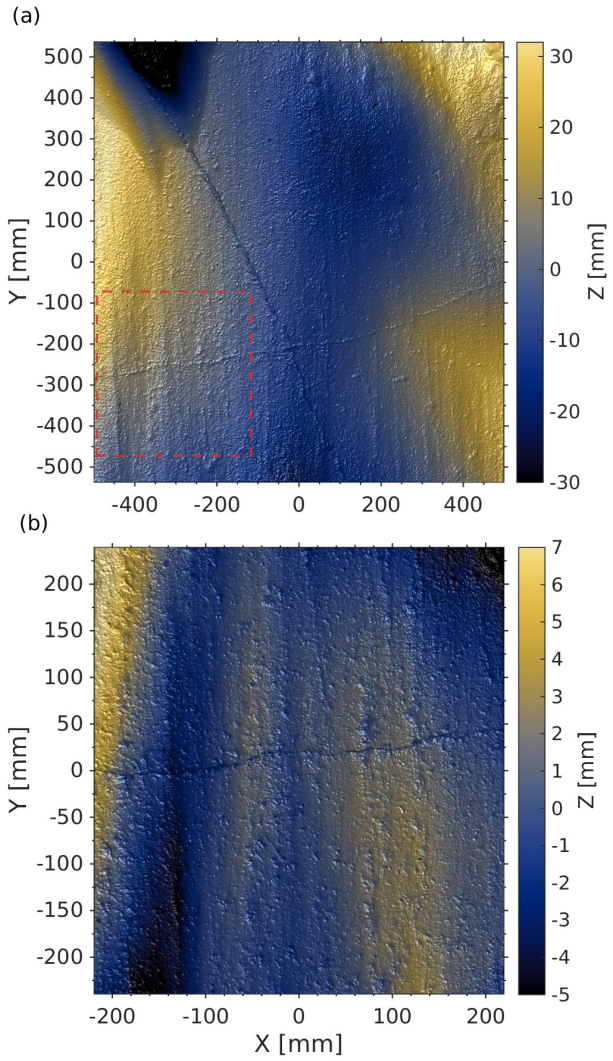

FIGURE 2. (color online) Rough interface results from a glacially abraded surface in (a) the low-resolution mode, and (b) the high-resolution mode. The glaciers flowed in the negative y direction. The color bar corresponds to height reference to the surface mean, and the brightness, or black/white information communicates the surface slope. The dashed box in (a) indicates the portion of the surface that is shown in (b).

More information on the measurements, as well as parameters extracted from the power spectra can be found in [1].

3.2. **Scattering Strength estimates from rock outcrops.** The sonar data analyzed was collected in April, 2011 during a joint field experiment that took place near Larvik, Norway, as part of a collaborative work with the Norwegian Defence Research Establishment (FFI). The SAS system operated at a center frequency of 100 kHz, has a bandwidth of 30 kHz and was operated from the HUGIN Autonomous Underwater Vehicle (AUV).

SAS images of a smooth, flat rock outcrop can be seen in Fig. 4 and is denoted R, and SAS images of four other rock outcrops can be seen in Fig. 5. These outcrops, called

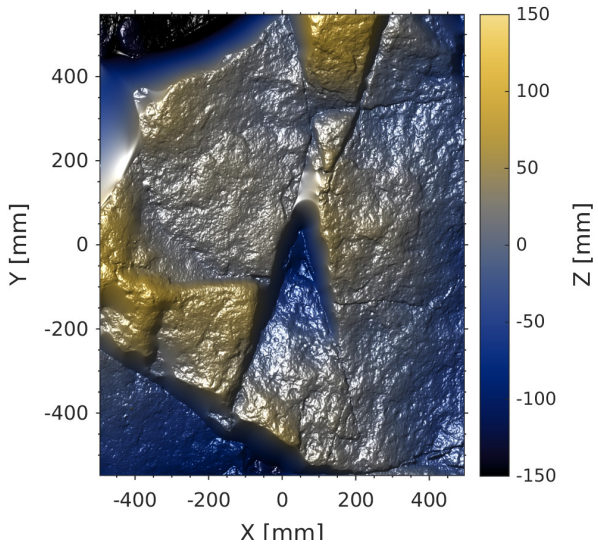

FIGURE 3. (color online) Roughness measurement results for the plucked rough interface. The colorscale communicates surface height, and the surface slope has been included as changes to grayscale value to accentuate low-amplitude roughness not resolved by the color scale. Only the low resolution measurement is presented because the high resolution mode does not include enough facets to obtain a proper sample size.

roches moutonees, were formed through glacial erosion and exhibit two contrasting roughness characteristics. The stoss side is formed through the mechanism of glacial abrasion [4] where the glacier flows up onto the outcrop and is characterized by a very smooth, polished surface at small scales, and a gently undulating surface at large scales. The leeward side is formed through the mechanism of glacial quarrying [5] where the glacier flows off of the outcrop and is characterized by a stepped appearance, where the step sizes and orientations result from the internal joint organization of the bedrock, at scales of O(1m) and small-scale isotropic roughness resulting from fracturing at small scales (O $<$ 0.1m). Boxes denote areas from which scattering strength was estimated, with blue boxes denoting areas of glacial abrasion and green boxes denoting areas of glacial plucking in Fig. 5.

From the Larvik, Norway, trial, estimates of scattering strength from abraded surfaces range between -33 and -26 dB, and scattering strength from quarried surfaces range between -30 and -20 dB. Scattering strength results are presented below, and compared to model curves. The measured scattering cross section from the plucked surfaces exhibited variability on the order of 5 dB. The abraded part of these outcrops has very low small-scale roughness, and it is likely that the scattering cross section measured on these sections can be predicted by first-order scattering models, such as the small-slope approximation (SSA). The plucked component of these outcrops has very large rms roughness compared to the wavelength, and it is likely that first-order scattering models cannot predict the scattering cross section.

From the Larvik, Norway, trial, scattering strength from rocks was extracted from the normalized pressure squared by selecting a region and averaging in cross-range, and then averaging over one degree increments. To measure the scattering strength from a rock surface, the mean slope was determined from high-resolution interferometric bathymetry so that the global grazing angle of the ideal mean seafloor could be mapped to the local

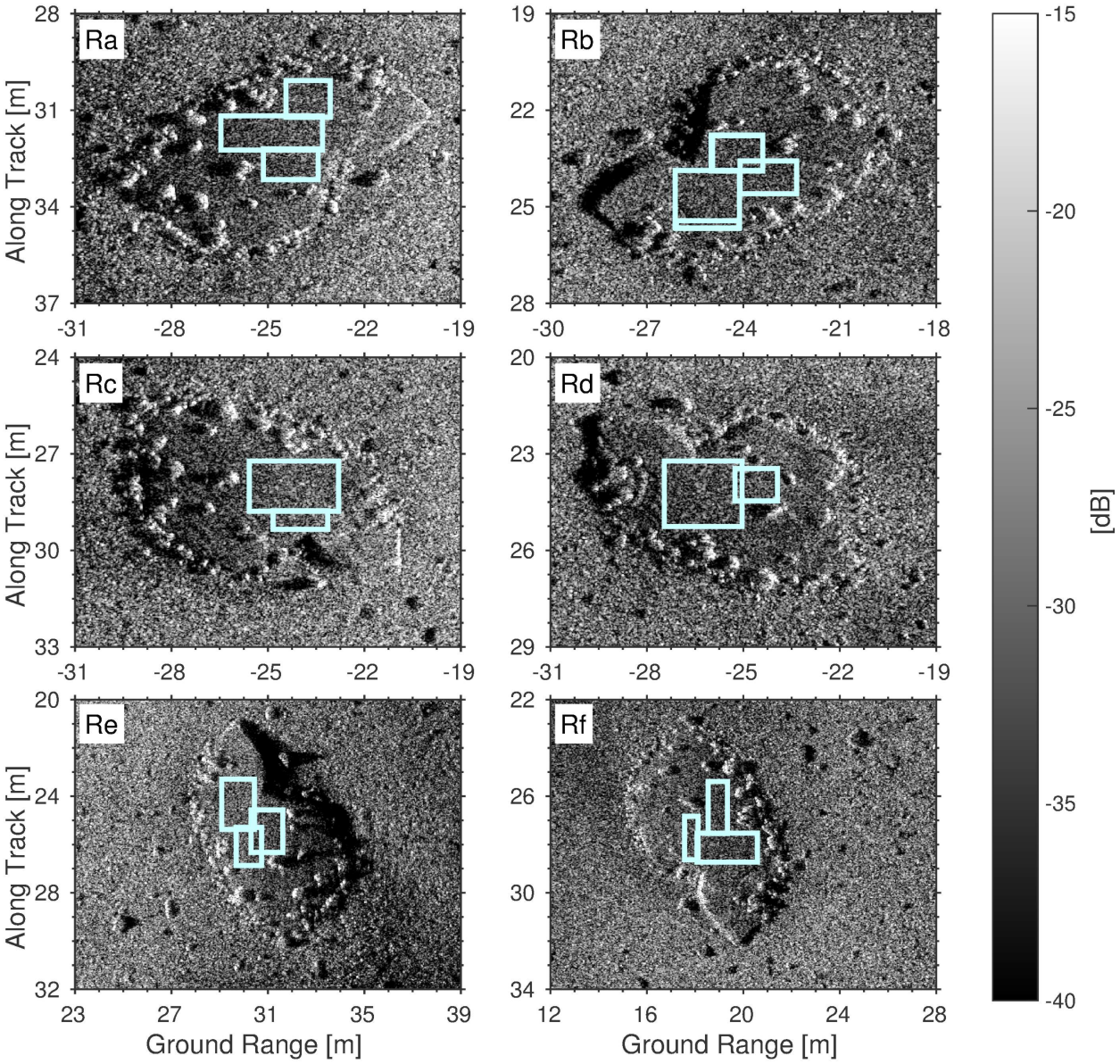

FIGURE 4. (color online) SAS images of the calibration rock outcrop. Boxes denote areas where pixels were extracted to form estimates of scattering strength. With respect to Ra, the rest of the images (Rb-Rf in order) are related in azimuth angle by the following counterclockwise rotations: 180°, 45°, 225°, 270°, and 390°. Grayscale value denotes the decibel equivalent of $\tilde{\sigma}$, the unaveraged scattering cross section. Horizontal axes represent ground range from the sonar track with positive values representing the port side, and negative values representing the starboard side. Vertical axes represent distance along the sonar track.

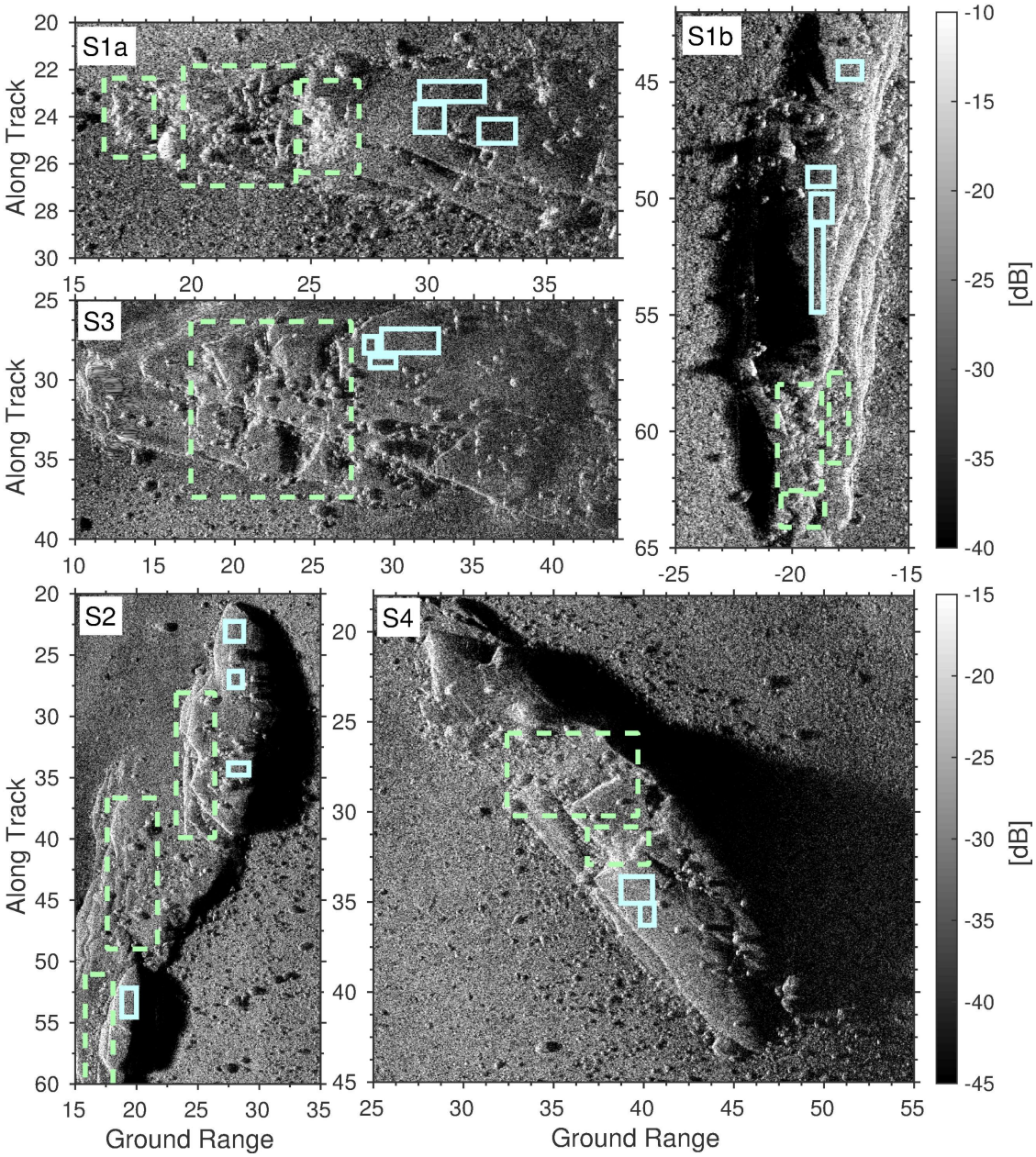

FIGURE 5. (color online) SAS images of *roches moutoneés*. Horizontal axes show ground range distance from the sonar track, with negative values corresponding to port, and positive corresponding to starboard. Vertical axes denote distance along the sonar track. Grayscale value corresponds to the decibel equivalent of $\tilde{\sigma}$, the unaveraged scattering cross section, and boxes outline areas where pixels were used to estimate scattering strength. Solid boxes indicate regions of glacial abrasion and dashed boxes indicate regions of glacial plucking.

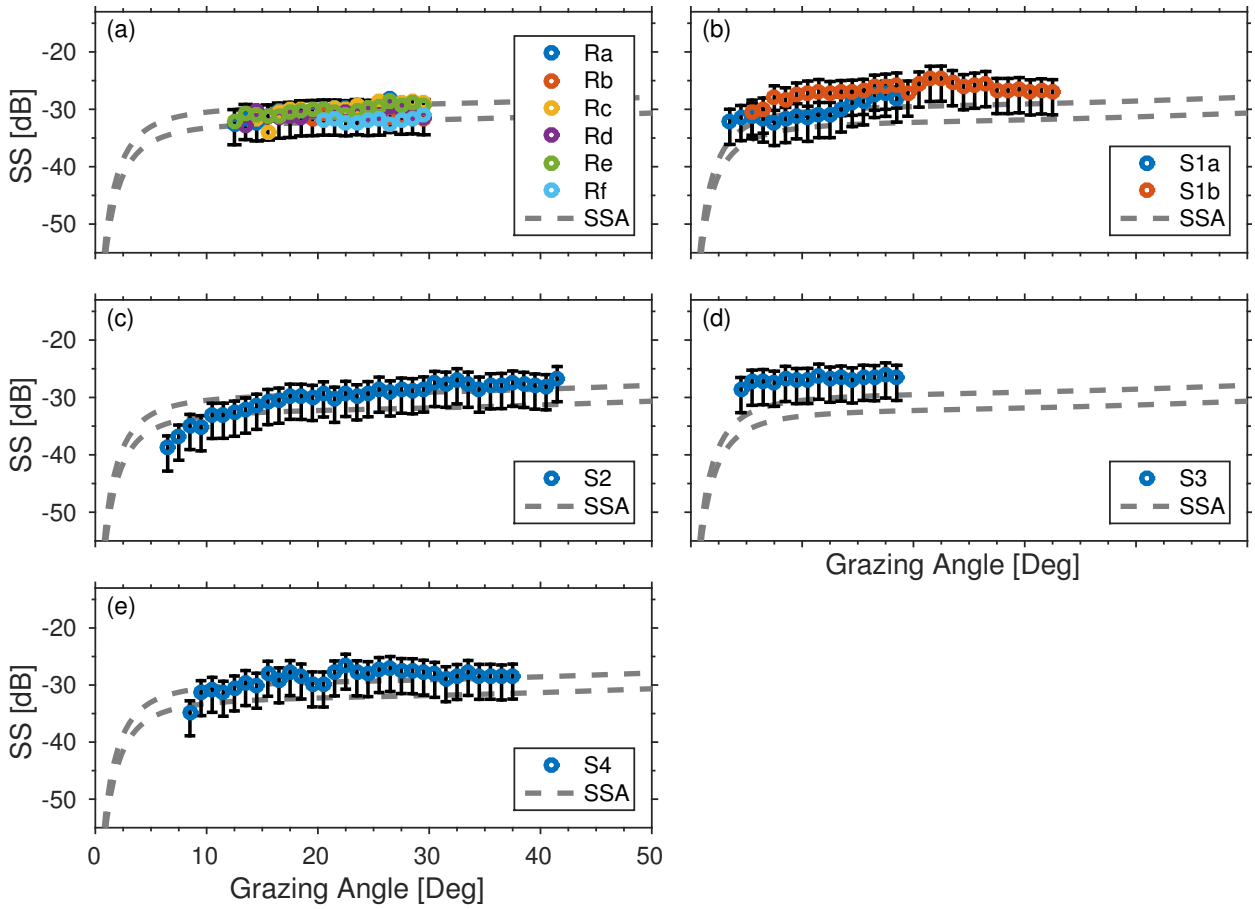

FIGURE 6. (color online) Scattering strength as a function of grazing angle from glacially abraded surfaces a) R, the calibration rock, b) S1, c) S2, d) S3, and e) S4. Error bars represent the measurement uncertainty, and the two gray dashed lines indicate the error bounds of the small slope approximation (SSA) due to uncertainty in input parameters.

grazing angle of the rock. Scattering strength results are presented in Fig. 6 for abraded surfaces and in Fig. 7 for plucked surfaces. After system calibration, scattering strengths from the low-amplitude roughness of the abraded side of the rock outcrops was found to range between -33 and -26 dB at 20 grazing angle, and agrees with predictions using the SSA with input parameters measured during the May 2013 experiment. This agreement is expected, since the rms height of abraded surfaces times the acoustic wavenumber is less than unity. Scattering strengths from the high-amplitude roughness of the plucked side ranged between -30 and -20 dB at 20 grazing angle. Predictions using small slope with measured parameters from the plucked interface resulted in an overestimate of 8 dB or more. This overestimate of scattering strength by a first-order model is unexpected, and indicates that higher-order modeling techniques may not yield acceptable predictions of scattering strength, due to the fact that higher-order terms in the cross section are typically positive-definite [6]. The composite roughness model [7] is hypothesized as a plausible way forward to predict the scattering cross section from faceted surfaces when using systems that have resolution smaller than the mean facet size.

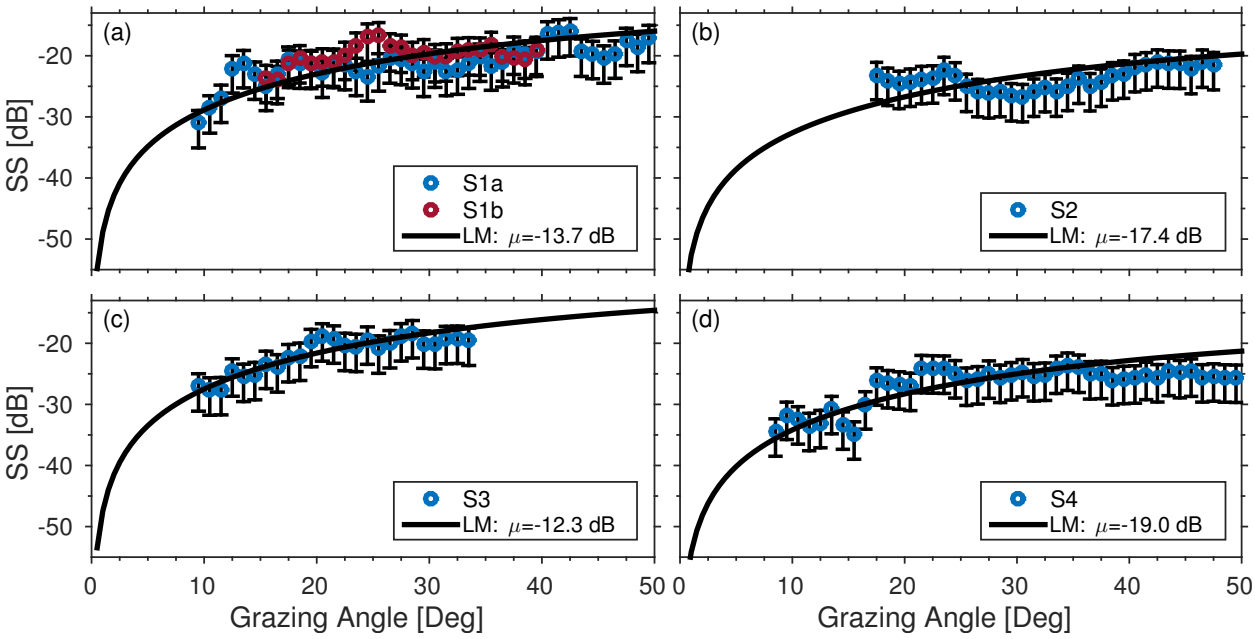

FIGURE 7. (color online) Scattering strength as a function of grazing angle from glacially plucked surfaces a) S1, b) S2, c) S3, and d) S4. Error bars represent the measurement uncertainty, and the black line represents the empirical Lambertian model (LM) with the parameter μ estimated by best-fit to the data.

3.3. **Scattering Statistics of rock outcrops.** The probability density function (PDF) of the magnitude of the scattered field is an important quantity for target detection systems. This quantity is typically expressed in terms of the probability of false alarm (PFA), which is equal to $1 - CDF$, where the CDF is the cumulative density function.

Analysis of the PFA from rock outcrops was performed during FY17 and modeled using a mixture model. The SAS images from wich PFA estimates were extracted are presented in Fig. 5. These images were calibrated during FY15 and FY16 of this project, and scattering strength estimates were obtained and documented in [1].

For this report, we will restrict attention to the rock outcrop S3 in Fig. 5. The PFA is estimated by extracting pixels within the green rectangles in Fig. 5, and binning them according to the large-scale slope available through SAS bathymetry. We focus on angles between 20 and 30 degrees grazing angle. The PFA from the S3 rock outcrop is shown in Fig. 8. The data is presented in the blue curve, and two models are comapred to it, a K-distribution [8], and a mixture model [9]. Although the measured PFA is quite heavy-tailed, the K distribution fails to capture the trends seen in the data. The K-distribution is commonly used to model patchy environments that behave like discrete scatterers, and the shape parameter is related to the effective number of scatterers per resolution cell.

However, examination of S3 in Fig. 5 shows that the scattered field is caused by several features 1) low amplitude scattering from horizontal facest, 2) high amplitude from vertical facets that may include multiple scattering from corners, and 3) small dropstones. If we assume that only the first two scattering sources dominate the scattered field, then a two-component mixture model for the scattered field envelope distribution has a plausible physical basis. Measurements of the PFA of rock outcrops with low amplitude roughness

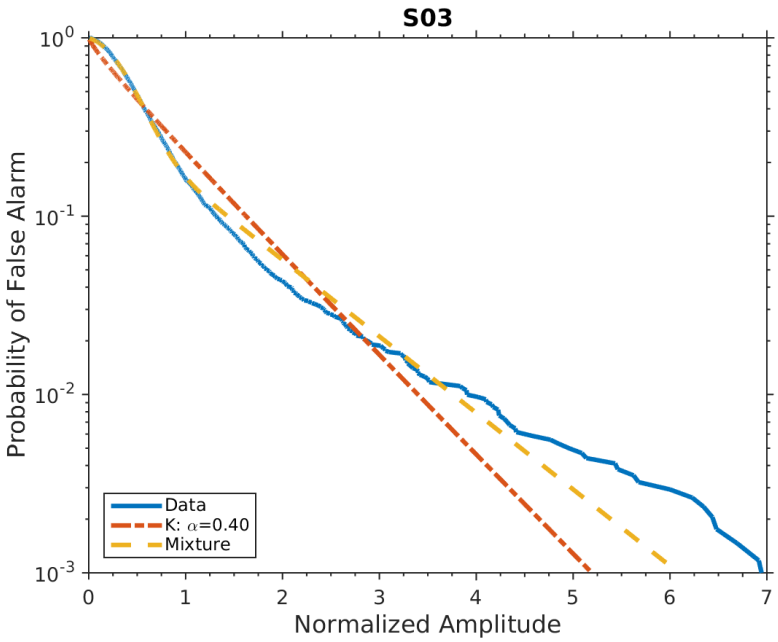

FIGURE 8. PFA of pixels bounded by green dashes of S3 in Fig. 5. The data are compared to both a K distribution and a two-component mixture model.

showed that the low amplitude scattering is adequately modeled using the Rayleigh distribution. Since there are a small number of bright vertical facets in the SAS image, it makes sense to use a K-distribution to model the high-amplitude component, because this distribution results from a small number of discrete scatterers.

The mixture model we use is specified by

$$p(x|\rho,\lambda_0,\alpha,\lambda) = \rho p_R(x|\lambda_0) + (1-\rho)p_K(x|\alpha,\lambda) \tag{1}$$

where the notation $p(y|a,b,c,\dots)$ is the pdf of random variable y with model parameters $a,b,c,\dots$, $p(x|\rho,\lambda_0,\alpha,\lambda)$ is the two-component mixutre model with four parameters, ρ is the relative proportion of samples folloing Rayleigh statistics, λ_0 is the scale parameter of the Rayleigh distribution, α is the shape parameter of the K-distribution, and λ is the scale parameter of the K-distribution. This two-component mixture distribution represents a combination of background (Rayleigh) and clutter (K) distrubitons, and was used to model midfrequency active reverberation data in [9].

The standard method to extimate mixture model parameters is called the Expectaction Maximization (EM) algorithm [9]. The EM algorithm proceeds in two stages. First if we have an initial guess of the model parameters, $\{\hat{\rho},\hat{\lambda_0},\hat{\alpha},\hat{\lambda}\}$, we can use those to assign weights to each data sample via

$$W_{0,i} = \frac{\hat{\rho}L_{0,i}}{\hat{\rho}L_{0,i} + (1-\hat{\rho}L_{1,i}} \tag{2}$$

$$W_{1,i} = 1 - W_{0,i} \tag{3}$$

$$L_{0,i} = p_R(X_i;\hat{\lambda_0}) \tag{4}$$

$$L_{1,i} = p_K(X_i;\hat{\alpha},\hat{\lambda}) \tag{5}$$

where $W_{0,i}$ is a weight that represents the belief that sample i belongs to the background Rayleigh distribution, $W_{1,i}$ is a weight that sample i belongs the clutter K distribution, $L_{0,i}$ is the likelihood function of the background component for sample i, $L_{1,i}$ is the likelihood function of the clutter component for sample i, and X_i is the ith data point. The weights provide a soft partition of the data into each of the mixture component distributions. The second step is to use these belief weights to improve our estimate of the mixture parameters by maximizing an intermediate function called the Q function for each component, which is the sum of the product of the log likelihood function for each distribution components and the weights. The Q function for the background component is

$$Q(\rho, \lambda_0) = \sum_{i=1}^{n} W_{0,i} \log(\rho) + \sum_{i=1}^{n} W_{0,i} \log(p_R(X_i, \lambda)) \tag{6}$$

and the Q function for the clutter component is

$$Q(\alpha, \lambda) = \sum_{i=1}^{n} W_{1,i} \log(p_K(X_i, \alpha, \lambda)) \tag{7}$$

Maximizing the Q function for the background Rayleigh component results in a closed form solution for $\hat{\rho}$ and $\hat{\lambda_0}$,

$$\hat{\rho} = \frac{1}{n} \sum_{i=1}^{n} W_{0,i} \tag{8}$$

$$\hat{\lambda} = \frac{1}{n\hat{\rho}} \sum_{i=1}^{n} W_{0,I} X_i \tag{9}$$

Maximizing the Q function for the clutter component typically requires a numerical algorithm, a few of which are suggested in [9]. In this work for the K clutter component, we use the weighted method of moments estimator instead of directly maximizing the Q function (as performed by [9]), and thus we call the EM algorithm employed in this work the EM-MoM. This discrepancy results in different parameter estimates between the Maximum Likelihood and EM-MoM estimates, discussed below.

These two steps (estimating the weights, and estimate the parameters) are repeated until some convergence criterion is met. The EM algorithm (software provided by Douglas Abraham of CausaSci LLC) was used to estimate model parameters that are plotted in Fig. 8.

The sequence of paremter estimates provided by EM can be proven to monotonically increase the likelihood function [10], although such a proof does not exist for EM-MoM. Such iterative algorithms can often become trapped in local maxima, and may not converge to the global maximum of the likelihood function.

Apart from the shortcomings of the EM-MoM algorithm listed above, the parameter estimates for the proposed mixture model can be thought of as random variables that are related to the random variables that describe the roughness properties of the rock outcrops. Although the roughness of the rock outcrop is deterministic, it is convenient to think of the roughness properties as random. Since the mixture model parameters can be linked via a scattering model to the roughness parameters, it may be possible to use the scattered field envelope distribution as an observable to remotely sense roughness properties of fractured

TABLE 1. Parameter estimates using expectation maximization, and maxim a posteriori

Parameter	EM Estimate	MAP Estimate
ρ	0.6526	0.6066
λ_0	0.2416	0.2001
α	0.4438	0.7533
λ	5.4046	2.5598
CBR	9.9304	9.6367

rock surfaces. For use in an inversion algorithm, it is vital to understand the joint distribution of the roughness parameters (which is linked to the joint distribution of mixture model parameters) to uncover correlations and possible degeneracies in the data. Although EM gives us parameter estimates, it does not tell us any information about the joint distribution of the mixture model parameters.

A Bayesian framework can provide such an estimate of the joint probability distribution of mixture model parameters. The posterior probability distribution (PPD) of the model parameters given the data is $p(\mathbf{m}, \mathbf{d})$, where $\mathbf{m}$ is a four component vector of model parameters, and $\mathbf{d}$ is an n component vector of data points. The PPD is the quantity we wish to estimate, and is related to the likelihood function by

$$p(\mathbf{m}, \mathbf{d}) = \frac{L(\mathbf{d}|\mathbf{m})p(\mathbf{m})}{Z} \tag{10}$$

where $p(\mathbf{m})$ is the prior distribution of the model parameters (we assume a bounded uniform distribution), $L(\mathbf{d}|\mathbf{m})$ is the likelihood function, and Z is the evidence, equal to the prior distribution of the data $p(\mathbf{d})$. The evidence normalizes the numerator in Eq. (10) and ensures that the PPD integrates to unity over the parameter space. The best parameter estimate in a Bayesian framework is the parameter set that maximizes the PPD, and is referred to as the maximum a posteriori (MAP) estimate. If the prior distribution is uniform and overlaps with the ML estimate, then the MAP and ML parameter estimates are the same. The use of bounded uniform prior distributions for the model parameters was motivated by both our lack of specific knowledge about the environment, and for comparing the EM estimates with ML estimates. Bounds of these uniform prior distributions have been obtained by examination of the data.

The PPD from the data set in Fig. 8 was estimated using an exhaustive technique, using 100 samples between the bounds of $\rho \in \{0, 0.8\}$, $\lambda_0 \in \{0.0120.26\}$, $\alpha \in \{9, 1.6\}$, and $\lambda \in \{0, 6\}$. The exhaustive search resulted in parameter estimates that can be found in Table 1, and are compared to the EM-MoM estimates. The MAP was found by taking the maximum over the 100 sample 4D parameter space as a coarse estimate. The coarse estimate was refined using a downhill simplex algorithm that terminated when the log-likelihood function increased by less than 10^{-8} from the previous estimate. The PPD in this case is a four-dimensional distribution and is not easily visualized. Instead, the 2D marginal distributions of the parameters are plotted in Fig. 9, where each subfigure plots a different combination of the integrated 2D marginal distribution. The MAP parameter estimates are shown as green solid lines, and the EM estimates are shown as dashed blue lines. Significant correlations are seen between the parameters of the mixture distribution. The one-dimensional marginal distributions are shown in Fig. 10.

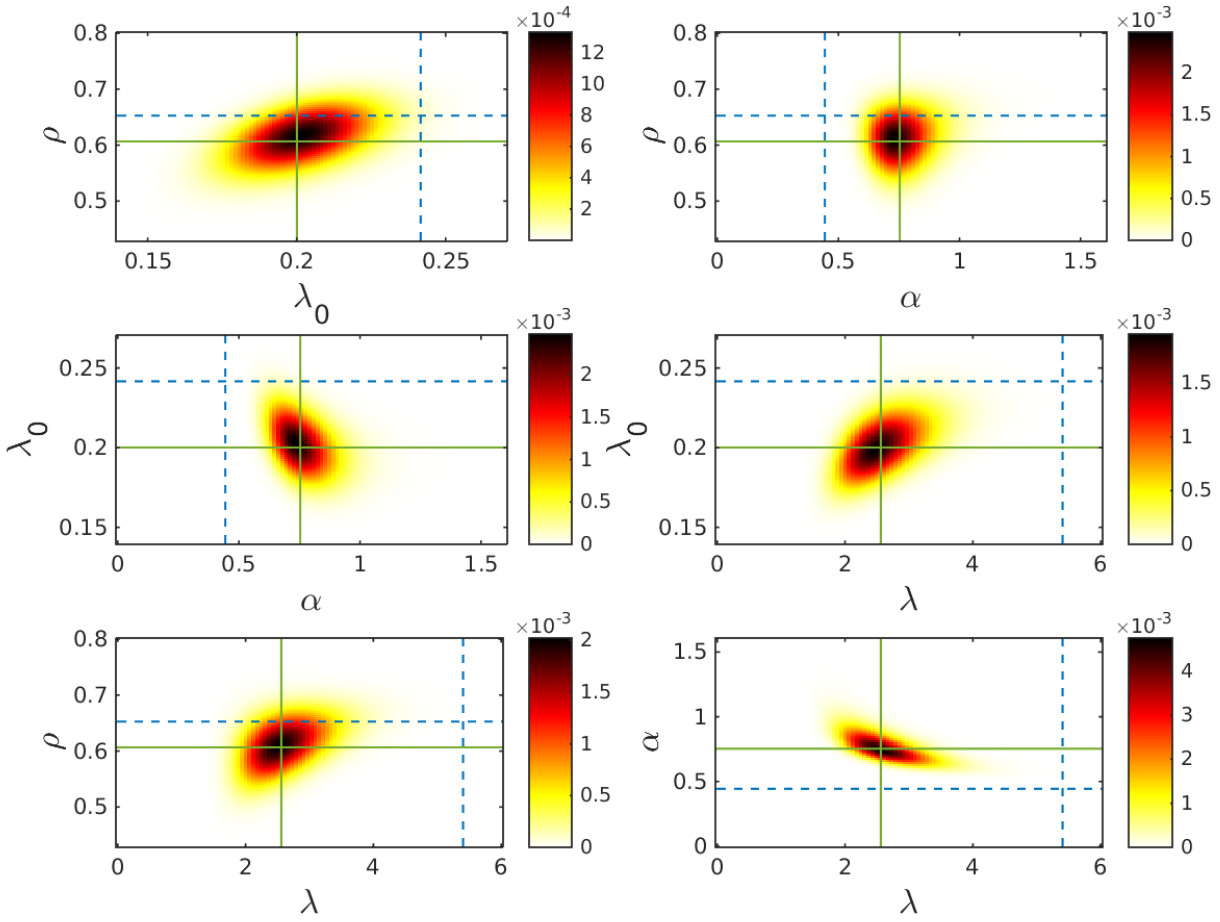

FIGURE 9. Joint marginal posterior probability distribution of the data in S3. These figures represent the full PPD integrated over two parameters, and is a convenient way to look at the full PPD with reduced dimensionality that we can visually interpret.

The resulting model PFAs from these estimates are plotted graphically in Fig. 11. The Rayleigh component of the mixture model is quite similar in both the EM and MAP estimates, although the tails are significantly different. The different estimates in the tails of the distribution are confirmed by the different estimates of the shape parameter for the EM-MoM estimate (about 0.5), and the MAP estimate (about 0.75). In the graphs of the PFAs in Fig. 11, the mixture model tails seem to be better estimated by EM than by MAP. The "clutter power" or variance of the clutter component for the K distribution is $\alpha\lambda$, and the "background power" or variance of the background component is λ_0. Therefore the clutter to background power ratio (CBR) is $\alpha\lambda/\lambda_0$, and is also included in Table. 1. For both EM -MoM and MAP estimates, the CBR is quite similar, even though the K distribution shape parameters are different.

We hypothesize that difference in estimates of α and λ are due to the method of moments estimator used in the maximization step of expectation maximization. The method of moments is not guaranteed to result in the same parameter estimates as maximum likelihood,

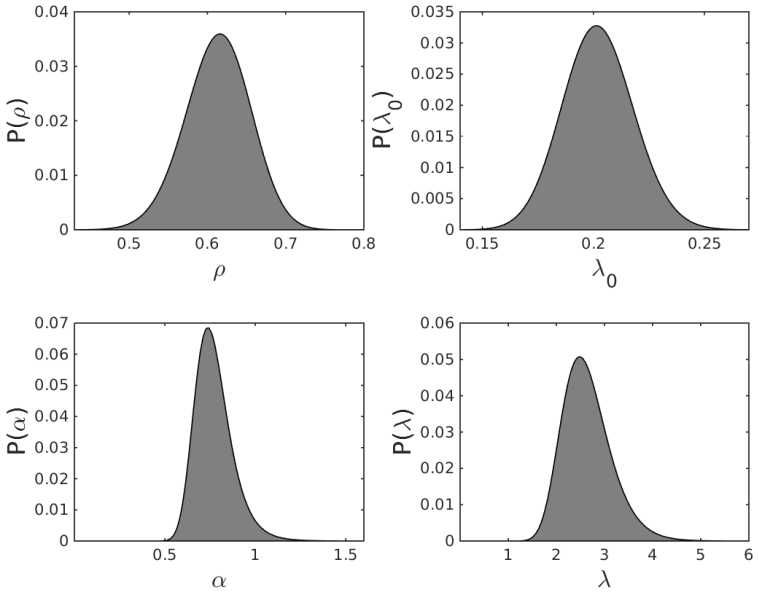

FIGURE 10. One dimensional marginal distributions of the parameters of the mixture model.

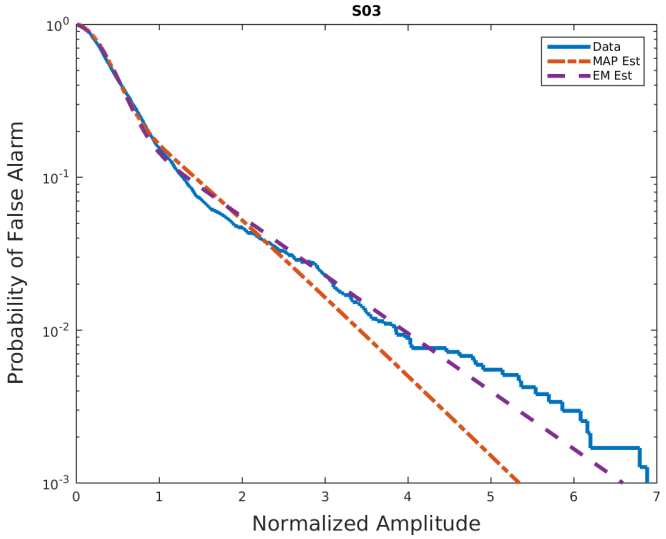

FIGURE 11. PFA plots of the envelope data from S3 compared to mixture model PFAs with parameters estimated using the Expectation Maximization algorithm, and MAP estimate from the Bayes framework. Note that the Rayleigh components of the both model estimates are similar, but the tails are significantly different.

and the repeated use of MoM over many iterations of the EM algorithm may cause the EM-MoM to diverge from the standard EM algorithm.

Therefore, although the EM-MoM algorithm does not necessarily maximize the true likelihood function of the mixture model, it provides a better estimate of the tails and at provides a similar CBR (at least for this example). In target detection systems, the distribution tails are the most problematic and cause a large number of false alarms. For inversion of roughness parameters using scattering statistics, the Bayes framework may be the most useful, although it is computationally expensive. For modeling false alarms in active sonar systems, the EM-MoM algorithm may be the best method to estimate parameters, and it is extremely fast compared to the full inversion for the PPD.

Future work in this area will focus on relating mixture model parameters to roughness statistics of the rock outcrop, including facet size distribution, and small-scale roughness power spectrum parameters. This physical model with enable forward modeling of target detection systems, performance prediction, and potential for remote sensing of the roughness properties of fractured rock outcrops. Comparisons of the mixture model parameter estimates using full-resolution SAS data and reduced resolution images that simulate target detection systems with poor angular resolution are key for modeling the performance of target detection systems.

4. Impact and Applications

The primary work completed over the course of this project consisted of developing techniques for modeling scattering from rough rock outcrop areas and comparing results with acoustic data sets collected from rocky areas. The proposed project was designed to increase our understanding of and simulation capability for acoustic scattering from rock outcrops. This study yielded useful knowledge of rock outcrops as a mechanism responsible for shallow water false alarms, and how levels of false alarm relate to physical properties and features of rock outcrops. Guidance relevant to this false alarm mechanism is being provided to researchers at the Naval Research Laboratory and will also be provided to those developing digital simulation content as part of other programs. Other deliverables are journal articles that have been published, and are in preparation.

We collaborated with researchers at NRL on their related project, "Modeling of High-Frequency Broadband False Target Phenomen" (project PIs were Roger Gauss, Dave Calvo, and Joe Fialkowski) as well as continuing the joint research project "Characterization and Modeling of Synthetic Aperture Sonar Data" with FFI (POC - Roy Hansen). The collaboration with NRL-DC resulted in two conference publications that will be presented at the OCEAN15 conference in October 2015 [11, 12].

References

[1] D. R. Olson, A. P. Lyons, and T. O. Sæbø, "Measurements of high-frequency acoustic scattering from glacially eroded rock outcrops," *J. Acoust. Soc. Am.*, vol. 139, no. 4, pp. 1833–1847, 2016.

[2] E.-R. Neumann, "Compositional relations among pyroxenes, amphiboles and other mafic phases in the Oslo Region plutonic rocks: Publication no. 115 in the Norwegian Geotraverse project," *Lithos*, vol. 9, no. 2, pp. 85 – 109, 1976.

[3] G. Mavko, T. Mukerji, and J. Dvorkin, *The Rock Physics Handbook: Tools for Seismic Analysis in Porous Media*. Cambridge, UK: Cambridge University Press, 2003.

[4] R. Alley, K. Cuffey, E. Evenson, J. Strasser, D. Lawson, and G. Larson, "How glaciers entrain and transport basal sediment: Physical constraints," *Quat. Sci. Rev.*, vol. 16, no. 9, pp. 1017 – 1038, 1997.

[5] B. Hallet, "Glacial quarrying: A simple theoretical model," *Ann. Glaciol.*, vol. 22, pp. 1 – 8, 1996.

[6] E. I. Thorsos and D. R. Jackson, "Studies of scattering theory using numerical methods," *Waves Random Media*, vol. 1, no. 3, pp. S165–S190, 1991.

[7] D. R. Jackson, D. P. Winebrenner, and A. Ishimaru, "Application of the composite roughness model to high-frequency bottom backscattering," *J. Acoust. Soc. Am.*, vol. 79, pp. 1410–1422, 1986.
[8] A. P. Lyons and D. A. Abraham, "Statistical characterization of high-frequency shallow-water seafloor backscatter," *J. Acoust. Soc. Am.*, vol. 106, pp. 1307–1315, 1999.
[9] D. Abraham, J. Gelb, and A. Oldag, "Background and clutter mixture distributions for active sonar statistics," *Oceanic Engineering, IEEE Journal of*, vol. 36, no. 2, pp. 231–247, April 2011.
[10] D. M. Titterington, A. M. Smith, and U. E. Makov, *Statistical Analysis of Finite Mixture Distributions*. Chichester, UK: John Wily and Sons, 1985.
[11] R. C. Gauss, J. M. Fialkowski, D. C. Calvo, R. Menis, D. R. Olson, and A. P. Lyons, "Moment-based method to statistically categorize rock outcrops based on their topographical features," in *OCEANS 2015 - MTS/IEEE Washington*, Oct 2015, pp. 1–5.
[12] D. C. Calvo, M. Nicholas, J. M. Fialkowski, R. C. Gauss, D. R. Olson, and A. P. Lyons, "Scale-model scattering experiments using 3d printed representations of ocean bottom features," in *OCEANS 2015 - MTS/IEEE Washington*, Oct 2015, pp. 1–7.